

K⁺ Currents in Isolated Vestibular Afferent Calyx Terminals

RITU DHAWAN¹, SCOTT E. MANN¹, FRANCES L. MEREDITH^{1,2}, AND KATHERINE J. RENNIE^{1,2,3}

¹*Department of Otolaryngology, University of Colorado Denver, Anschutz Medical Campus, 12700 E. 19th Avenue, MS 8606, Aurora, CO 80045, USA*

²*Neuroscience Program, University of Colorado Denver, Anschutz Medical Campus, 12800 E. 19th Avenue, MS 8315, Aurora, CO 80045, USA*

³*Department of Physiology and Biophysics, University of Colorado Denver, Anschutz Medical Campus, 12800 E. 19th Avenue, MS 8307, Aurora, CO 80045, USA*

Received: 24 April 2009; Accepted: 4 March 2010; Online publication: 21 April 2010

ABSTRACT

Vestibular hair cells transduce mechanical displacements of their hair bundles into an electrical receptor potential which modulates transmitter release and subsequent action potential firing in afferent neurons. To probe ionic mechanisms underlying sensory coding in vestibular calyces, we used the whole-cell patch-clamp technique to record action potentials and K⁺ currents from afferent calyx terminals isolated from the semicircular canals of Mongolian gerbils. Calyx terminals showed minimal current at the mean zero-current potential (−60 mV), but two types of outward K⁺ currents were identified at potentials above −50 mV. The first current was a rapidly activating and inactivating K⁺ current that was blocked by 4-aminopyridine (4-AP, 2.5 mM) and BDS-I (up to 250 nM). The time constant for activation of this current decreased with membrane depolarization to a minimum value of ~1 ms. The 4-AP-sensitive current showed steady-state inactivation with a half-inactivation of approximately −70 mV. A second, more slowly activating current (activation time constant was 8.5±0.7 ms at −8 mV) was sensitive to TEA (30 mM). The TEA-sensitive current also showed steady-state inactivation with a half-inactivation of −95.4±1.4 mV, following 500-ms duration conditioning pulses. A combination of 4-AP and TEA blocked ~90% of the total outward current.

Correspondence to: Katherine J. Rennie · Department of Otolaryngology · University of Colorado Denver · Anschutz Medical Campus, 12700 E. 19th Avenue, MS 8606, Aurora, CO 80045, USA. Telephone: +1-303-7243070; fax: +1-303-7244553; email: katie.rennie@ucdenver.edu

In current clamp, single Na⁺-dependent action potentials were evoked following hyperpolarization to potentials more negative than the resting potential. 4-AP application increased action potential width, whereas TEA both increased the width and greatly reduced repolarization of the action potential.

Keywords: semicircular canals, KCNQ, hair cells, BDS-I

INTRODUCTION

The sensory hair cells of the vestibular system convert displacement-driven hair bundle motion into electrical activity of primary vestibular afferents. In mammalian, reptilian, and avian species, there are type I and type II hair cells which differ in several respects including their innervation characteristics. Whereas bouton afferents make synaptic contact with a small portion of the type II hair cell basolateral membrane, calyx-shaped afferent terminals engulf the basolateral surface of one or more type I hair cells (Wersäll 1956). How the calyceal synapse operates remains enigmatic. Detection of excitatory postsynaptic currents (EPSCs) in solitary gerbil calyces (Rennie and Streeter 2006) and CNQX-sensitive potentials in turtle vestibular afferents support α -amino-3-hydroxy-5-methyl-4-isoxazolepropionic acid (AMPA)-mediated quantal transmission at this synapse (Bonsacquet et al. 2006; Holt et al. 2007a). Furthermore, in common with other hair cells from the auditory and vestibular systems,

there are several ribbon synapses within type I hair cells and their calyces which provide the synaptic machinery for chemical neurotransmission (Lysakowski and Goldberg 1997). However, calyx endings make several invaginations into the type I hair cell where the intercellular cleft narrows to 6–7 nm (Gulley and Bagger-Sjöback 1979). The close arrangement between the presynaptic type I hair cell and its postsynaptic calyx has driven speculation that other less conventional modes of transmission may also occur at this synapse (Goldberg 1996), and recent evidence shows that driven voltage changes in the membrane potential of calyx-bearing afferents persist even in the presence of glutamate receptor antagonists (Holt et al. 2007a).

The afferent innervation patterns of hair cells in the vestibular neuroepithelium are complex. Some vestibular primary afferents, known as calyx fibers, receive input from type I hair cells and only have calyx terminals. Other vestibular afferents, known as dimorphic fibers, receive input from both hair cell types and have calyceal and bouton terminals. In a third type of configuration, bouton fibers receive their sole input from type II hair cells and only have bouton terminals. The three afferent classes differ in their electrophysiological properties (Baird et al. 1988; Fernández et al. 1988). Calyx fibers have a larger diameter and fire action potentials that are irregularly spaced and have a relatively low gain in response to rotational stimuli compared to dimorphic and bouton terminals (Baird et al. 1988; Lysakowski et al. 1995). Bouton terminals show a regular firing pattern and tonic response dynamics in response to acceleration, and dimorphic fibers have properties that are intermediate between irregular and regular neurons. The mechanisms underlying these differences are not clear, but differences in neuronal membrane conductances are likely to contribute. In cultured rat primary vestibular neurons, a high conductance calcium-dependent K⁺ channel (BK) was found to contribute to afferent firing characteristics (Limón et al. 2005). In vestibular ganglion neurons from early postnatal mice and rats, voltage-activated K⁺ currents with differential sensitivities to 4-AP and TEA have been identified (Chabbert et al. 2001; Risner and Holt 2006; Iwasaki et al. 2008). In ganglion preparations, the terminal innervation characteristics of the neurons were not known.

In this study, we have made patch-clamp recordings of whole-cell K⁺ currents in calyx terminals non-enzymatically dissociated from the semicircular canals of Mongolian gerbils. Calyx terminals were isolated together with associated type I hair cells. We found a rapidly activating and inactivating current sensitive to 4-AP and BDS-I and a slower inactivating current sensitive to relatively high concentrations of TEA. We also investigated the influence of the TEA- and 4-AP-

sensitive K⁺ conductances on action potentials in current clamp to address the function of K⁺ channels in isolated calyces.

METHODS

Cell preparation

Calyx terminals were dissociated along with type I hair cells using methods outlined previously (Rennie and Streeter 2006). Animal procedures were performed under protocols approved by the University of Colorado's Institutional Animal Care and Use Committee and adhered to guidelines established by the American Physiological Society. Mongolian gerbils (*Meriones unguiculatus*, postnatal day 13 up to 12 weeks old, 10–90 g) were injected with pentobarbital sodium (Nembutal, 50 mg/kg ip) and ketamine (40 mg/kg im). The ampullae of the semicircular canals were surgically removed under deep anesthesia after opening up the bony labyrinth. Animals were decapitated immediately following canal removal. The six ampullae were immersed in “high-magnesium/low-calcium” saline containing (in millimolar): NaCl (135), KCl (5), MgCl₂ (10), CaCl₂ (0.02), HEPES (10), and D-glucose (3), pH 7.4 with NaOH and osmolality of 300–305 mmol/kg. The tissue was subsequently incubated for 32 min at 37°C and then transferred to a solution of Leibovitz's L-15 medium containing bovine albumin (0.5–1 mg/ml) for at least 50 min at room temperature (18–24°C) to reduce endogenous enzyme activity. Ampullae were then placed in standard L-15 medium (osmolality adjusted to 300–305 mmol/kg with distilled H₂O, pH 7.4–7.6) on a glass coverslip of the recording chamber, and the epithelial surface was stroked with a probe to dislodge cells. Cells were subsequently viewed on an Olympus upright microscope (BX50WI) equipped with water immersion objectives and differential interference contrast optics. Isolated type I hair cells were amphora-shaped and could be identified by a constricted neck region as described previously (Ricci et al. 1997). A camera (Oly 150, Olympus or T-Q/MM-8, Micro-Mac), mercury lamp (Olympus), and Lucifer Yellow filter set were also used in image acquisition. Images were recorded to videotape, converted to digital pictures using Moviestar 5 (SCM Microsystems, Fremont, CA), and merged using Paint Shop Pro (Corel, Ottawa, Canada). Cup-shaped calyx terminals were observed surrounding the basolateral regions of one and occasionally two or three type I hair cells. This is consistent with observations in fixed tissue from the gerbil crista ampullaris, where most calyces were single, but in some cases contacted up to four type I hair cells (Desai et al. 2005). Afferent stalks connected to calyces were almost never observed in isolated terminals. If a stalk was present, it is noted in the figure legend. All of

the electrophysiological data presented were from single calyces in contact with a single type I hair cell, except for one calyx which engulfed two type I hair cells.

Electrophysiological recording and solutions

A Sutter Instruments horizontal micropipette puller (Flaming/Brown P-87, Novato, CA, USA) was used to pull patch pipettes from capillary glass tubing (Warner Instrument Corp., Hamden, CT, USA, glass PG165T, outer diameter 1.65 mm, inner diameter 1.28 mm). Pipettes were fire-polished on a microforge (Narishige MF 83) and coated with silicone elastomer (Sylgard, Dow Corning) close to the tip to minimize capacitive transients. The normal patch pipette solution used in the majority of experiments comprised (in millimolar): KF (110), KCl (15), NaCl (1), HEPES (10), D-glucose (3), MgCl₂ (1.8), and ethylene glycol tetraacetic acid (EGTA) (10), pH 7.4 with KOH (~27 mM). Later recordings included 2 mM Na₂ATP in the patch electrode solution; this did not produce measurable differences in recorded currents. We also recorded from two cells with a solution containing (in millimolar): K gluconate (145), NaCl (2), HEPES (10), D-glucose (3), MgCl₂ (2), EGTA (5), MgATP (2), and LiGTP (0.2), pH 7.4 with KOH (18 mM). These

cells showed inward and outward currents with similar amplitudes and kinetics as seen with the KF/KCl pipette solution. For the images shown in Figure 1, cells were patched with an electrode solution comprising (in millimolar): KF (135), KOH (26), HEPES (10), D-glucose (3), MgCl₂ (2), EGTA (10), and Lucifer Yellow (dipotassium salt) (1.9), pH 7.4, in order to visually confirm whole-cell recordings using fluorescent dye.

Conventional whole-cell tight-seal patch-clamp experiments were carried out at room temperature (18–24°C). Currents were amplified with an Axo-patch-1D patch amplifier (Axon Instruments, Foster City, CA, USA) connected to a PC through an AD converter (Digidata 1320A, Axon Instruments) and using Clampex 8 software. The patch pipette had an open-tip resistance ranging from 1.0 to 4.5 MΩ and was placed in contact with the outer face of the calyx, usually close to the base of the hair cell in order to obtain a gigaseal. Whole-cell access was obtained using voltage pulses or negative pressure. Recordings were made from cells up to 6 h following mechanical dissociation of the cristae.

Signals were low-pass filtered online at 2 or 5 kHz, and the sampling rate was set between 10 and 20 kHz according to the protocol. Residual series resistance

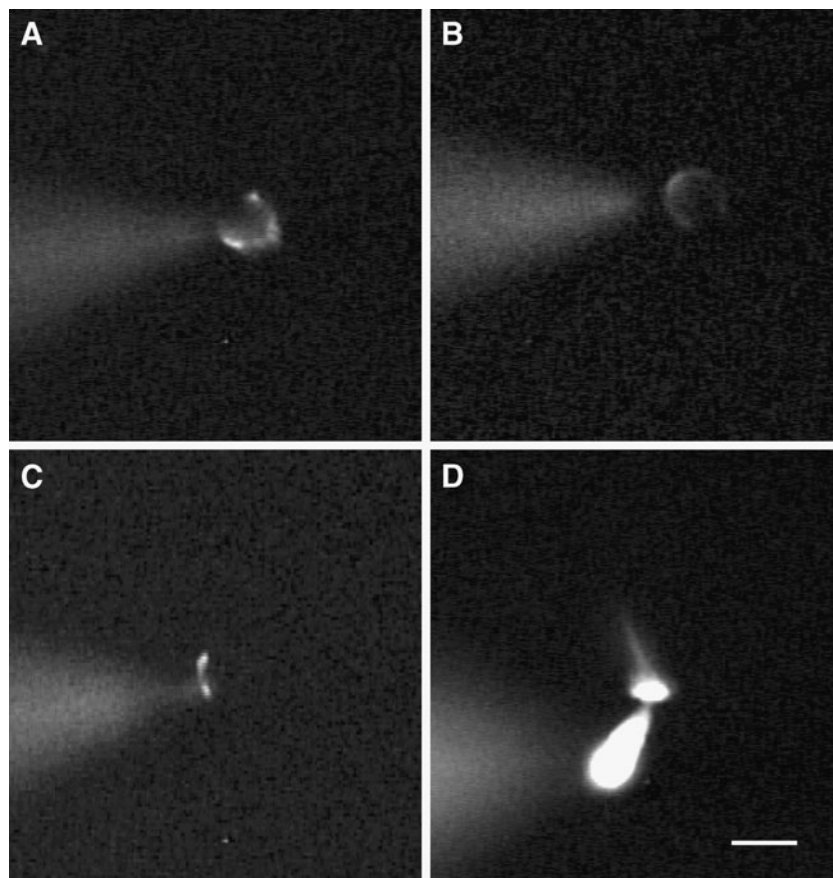


FIG. 1. Morphology of calyx terminals and type I hair cells as shown by the fluorescent dye Lucifer Yellow, which was included in the patch electrode solution. **A–C** Images of different calyx terminals surrounding type I hair cells that were loaded with the fluorescent dye during whole-cell recordings. Calyces in **A** and **B** appear as horseshoe-shaped structures which surrounded the basolateral regions of the associated hair cell, whereas in **C** the terminal was more restricted to the base of the type I hair cell. **D** A type I hair cell loaded with Lucifer Yellow showing the cell body, cuticular plate, and hair bundle. In each image, the dye containing patch electrode is seen to the left of the cell in a different focal plane. Scale bar represents 10 μm.

after compensation (0–70%) was $2.51 \pm 0.20 \text{ M}\Omega$ ($n=88$) and was not corrected further. Voltages were corrected off-line for liquid junction potentials between electrode and bath solutions. The mean input capacitance (C_m) for calyces was $3.73 \pm 0.18 \text{ pF}$ ($n=88$). No leak subtraction was performed.

In most experiments, the extracellular solution was L-15 medium. For Na⁺ replacement experiments, an extracellular solution containing (in millimolar): choline chloride (140), KCl (5), MgCl₂ (1.8), CaCl₂ (1.3), HEPES (10), and D-glucose (3), pH 7.4 with KOH was used and replaced a solution with the same ingredients except that, instead of choline, 140 mM NaCl was present. Chemicals were obtained from Sigma-Aldrich (St. Louis, MO, USA). Solutions containing drugs were applied locally to cells using gravity-fed flow pipes. For TEA experiments (when the TEA concentration exceeded 10 mM), TEA replaced an equimolar amount of Na⁺ or choline, except for experiments in current clamp where TEA was added to the L-15 solution. In other experiments, 4-AP, BDS-I (from a 4 μM stock solution in distilled water), or concentrations of TEA up to 10 mM TEA were added to the external solution, and the pH was adjusted to between 7.4 and 7.5.

Data analysis

Electrophysiological analyses were performed and figures generated using pClamp (8.1 and 8.2, Axon Instruments) and Sigmaplot (Jandel Scientific, v 8 or 11). Values presented are means ± standard errors of the mean (SEM) unless stated otherwise. Significance was determined with Students' *t* test using Sigmaplot software (Jandel Scientific v 2). In current clamp experiments, an action potential was defined as a voltage spike with a rapid upward inflection and amplitude greater than 45 mV above threshold. Input resistance values were calculated from voltage clamp data using a linear regression of a voltage vs. current plot at potentials between −90 and −60 mV following a 40-ms test pulse to −128 mV.

Steady-state inactivation curves for K⁺ currents were obtained using voltage protocols with either 150- or 500-ms prepulses from a holding potential of −78 mV, and resulting data were fitted with a Boltzmann function of the form

$$I/I_{\text{max}} = 1/1 + \exp[(V - V_{1/2})/S] \quad (1)$$

where V is the conditioning potential, $V_{1/2}$ is the half-maximum inactivation potential, and S determines the slope factor for inactivation. The activation and inactivation time course of currents were each fitted with a single exponential. Specifically, the activation

and inactivation of currents in Figure 5 were fitted according to

$$i(t) = a_1 e^{-t/\tau_1} + a_2 e^{-t/\tau_2} + b_1 \quad (2)$$

where a_1 and a_2 scale the relative activation and inactivation time courses, τ_1 and τ_2 are the time constants of activation and inactivation, and b_1 is the final steady-state current.

RESULTS

Verification of whole-cell recordings

Type I hair cells were isolated and identified as described previously, and in some cases a calyx terminal remained attached to the basolateral region of the type I hair cell (Rennie and Streeter 2006). In order to better visualize cells during whole-cell recordings, we carried out experiments using patch electrodes filled with electrode solution that included the fluorescent dye Lucifer Yellow. Gigaseals were made onto the outer face of calyces surrounding type I hair cells, and cell fluorescence was recorded following membrane breakthrough. Figure 1A–C shows examples of fluorescent calyces dialyzed with Lucifer Yellow. We recorded whole-cell currents from eight calyces filled with Lucifer Yellow electrode solution, and the currents recorded were similar to those seen with normal electrode solution, as shown for example in Figure 3A. Fluorescent calyx terminals were typically seen as a horseshoe-shaped structure (Fig. 1A, B) which surrounded the basolateral membrane around the type I hair cell. We used the same intracellular solution to make patch-clamp recordings from isolated type I hair cells as shown in the example of Figure 1D.

Whole-cell access to a type I hair cell was apparent from fluorescence in the hair cell and hair bundle (Fig. 1D) and the very low-input resistance which ranged from 40 to 155 MΩ (mean value $109 \pm 30 \text{ M}\Omega$, $n=10$) in type I hair cells (Fig. 2A). The low-input resistance can be attributed to the large resting K⁺ conductance that has previously been characterized in type I cells (Rennie et al. 1996; Chen and Eatock 2000). Unlike type I hair cells, calyx terminals did not have a large resting conductance and the mean input resistance was $735 \pm 183 \text{ M}\Omega$ ($n=8$). This was similar to input resistance values for calyces patched with normal electrode solution without Lucifer Yellow dye, where the mean value was $1.18 \pm 0.11 \text{ G}\Omega$ ($n=26$), and two cells patched with K gluconate solution whose input resistance values were 0.4 and 1.3 GΩ. Mean peak outward currents were also larger in type I hair cells as compared to calyces as seen in the current voltage (I - V) plots in Figure 2B.

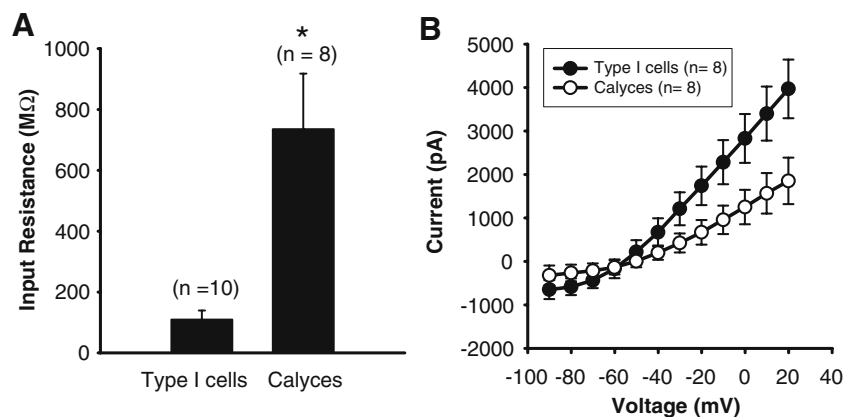


FIG. 2. Type I hair cells and calyx nerve terminals differ in input resistance and peak currents. The electrode solution contained Lucifer Yellow to visualize cells. **A** The mean input resistance in type I hair cells was $109 \pm 30 \text{ M}\Omega$ ($n=10$). In contrast, the mean input resistance in calyces was $735 \pm 183 \text{ M}\Omega$ ($n=8$). A *t* test revealed that

the two groups were significantly different. Asterisk denotes a *p* value < 0.01 . **B** Peak currents were on average consistently larger in type I hair cells as shown in the current-voltage plots. Mean values \pm SEM are shown for eight type I cells (filled symbols) and eight calyces (unfilled symbols).

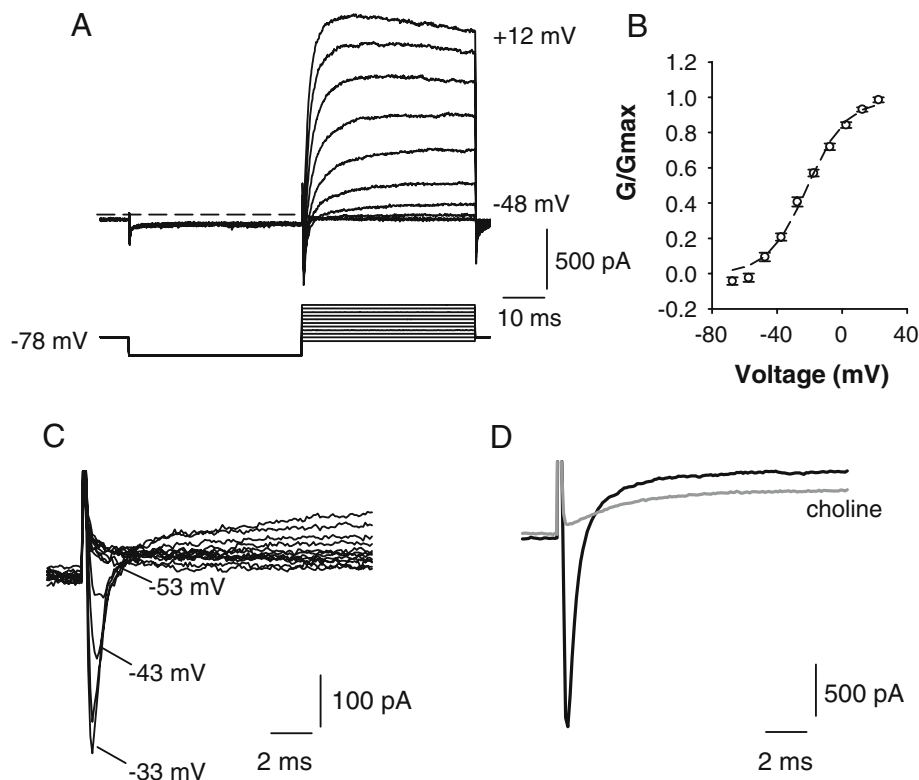


FIG. 3. **A** Typical whole-cell currents (upper) recorded from a calyx terminal in extracellular L-15 solution. Voltage protocol is shown in the lower panel. The cell was held at -78 mV and given a 40-ms hyperpolarizing pulse to -128 mV before stepping to test potentials in 10-mV increments between -88 and 12 mV . Dashed line indicates zero-current potential. **B** Plot showing activation of the peak outward current (G/G_{max}) as a function of membrane potential for nine cells (mean \pm SEM). A single Boltzmann fit to the data gave a half-activation of $-21.3 \pm 1.8 \text{ mV}$ and *S* value of $11.9 \pm 1.4 \text{ mV}$. **C** A rapid transient inward current typically preceded the slower outward

currents and was first seen at potentials more positive than -53 mV . Currents in response to 5-mV voltage steps between -88 and -33 mV are shown. Cell was stepped to -128 mV for 40 ms before each step to remove Na⁺ current inactivation. **D** Transient inward current in another calyx was abolished by replacement of external Na⁺ with choline (gray trace), confirming that inward currents were carried by Na⁺. Outward current was also reduced when the external Na⁺ was replaced with choline (gray trace). Test potential = -28 mV using the same voltage protocol as shown in **A**.

Whole-cell currents in calyx terminals

Whole-cell currents in calyx terminals were elicited in voltage clamp with depolarizing steps between -88 and 12 mV as shown in Figure 3A. Compared with voltage steps from a holding potential of -78 mV, outward currents were larger if a conditioning step to a more hyperpolarized potential was first given. We therefore used a standard protocol where steady-state inactivation of outward currents was removed by stepping the membrane to potentials of -120 mV or more negative for 40 ms before the test pulse (Fig. 3A, lower panel). The relative activation of the outward current is shown in Figure 3B. The mean half-activation of the macroscopic outward current was -21.3 ± 1.8 mV and S was 11.9 ± 1.4 mV ($n=9$). In most recordings, outward currents were preceded by transient inward currents at steps to potentials above approximately -50 mV. Inward currents are shown for 5-mV increment voltage steps between -88 and -33 mV in Figure 3C. We have previously shown that these transient inward currents are Na⁺ currents which are almost completely eliminated by 100 nM tetrodotoxin (Rennie and Streeter 2006). Substitution of the external Na⁺ with choline also abolished the transient inward current in six calyces. An example is shown in Figure 3D. This indicates that inward Ca²⁺ currents were not contributing to the rapid transient inward current. A T-type Ca²⁺ current has been

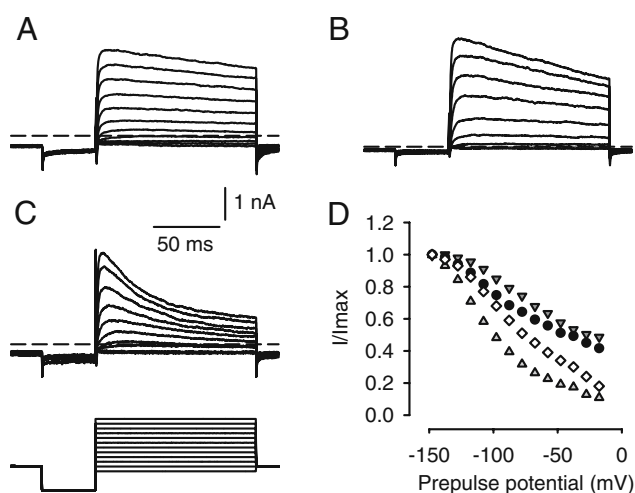


FIG. 4. Variation in inactivation properties of outward K⁺ currents. Examples of outward currents in three different calyces are shown in A–C. The voltage protocol was the same for all cells and is shown in the lower panel of C. Cells were held at -78 mV, prepulsed to -128 mV, and stepped to a range of voltages between -88 and 22 mV in 10-mV increments. Dashed line indicates zero-current potential. Scale bars in A apply to B and C also. D Inactivation expressed as a fraction of peak current (I/I_{\max}) is shown for four different cells (indicated by different symbols). Currents were measured at peak and 120 ms from the start of the test pulse to -8 mV following 40-ms prepulses to the potentials shown.

reported previously in mouse vestibular neurons during embryonic development, but its expression declines markedly after birth (Chambard et al. 1999; Autret et al. 2005). Interestingly, replacing the external Na⁺ with choline solution also produced a reduction in the outward current (Fig. 3D). In five cells tested, the peak outward current was reduced by a mean value of $24.7 \pm 4.4\%$ in extracellular choline solution. The reduction in outward current was not investigated further here, but a similar effect has been described previously in cultured primary afferent vestibular ganglion neurons (Soto et al. 2006). In that preliminary study (Soto et al. 2006), an outward K⁺ current was reduced when external Na⁺ was replaced with choline, and the effect was attributed to Na⁺-activated K⁺ channels (K_{Na}) (Bhattacharjee and Kaczmarek 2005).

Outward currents in calyx terminals activated above approximately -50 mV (Figs. 2B and 3B). The mean peak amplitude of the outward current measured at ~ 0 mV in the normal extracellular solution (L-15) was 1.40 ± 0.09 nA ($n=88$). We previously reported that replacement of K⁺ with Cs⁺ in the electrode solution blocked the outward currents, indicating that they were K⁺ currents (Rennie and Streeter 2006). During 120-ms duration test pulses, outward currents in calyces always showed some degree of time-dependent inactivation at depolarized potentials. The extent of current inactivation varied between calyces as shown in Figure 4. The cell shown in Figure 4A showed only a small degree of current inactivation, the cell in Figure 4B showed more inactivation, and the cell in Figure 4C showed the greatest amount of inactivation during 120-ms duration steps. We assessed the inactivation as the current magnitude at the end of the pulse divided by the peak current during a step to 2 mV and found a mean value of $64.2 \pm 3.6\%$ ($n=41$ calyces). The steady-state inactivation of outward current as a function of prepulse potential is shown for four cells in Figure 4D. The variability in inactivation between calyces suggests heterogeneity in the expression of underlying K⁺ channels. We therefore further dissected the inactivating current using different K⁺ channel blockers as follows.

4-AP block of outward K⁺ currents in calyx terminals

The effects on the outward current of increasing concentrations of the K⁺ channel blocker 4-AP are shown in Figure 5A. At an extracellular concentration of 0.25 mM, 4-AP reduced the total outward current at the end of a 40-ms step by $\sim 25\%$. As shown in the I - V relations in Figure 5B, peak outward currents were increasingly blocked at potentials above -40 mV as the 4-AP concentration was raised from 0.25 to 0.75 mM

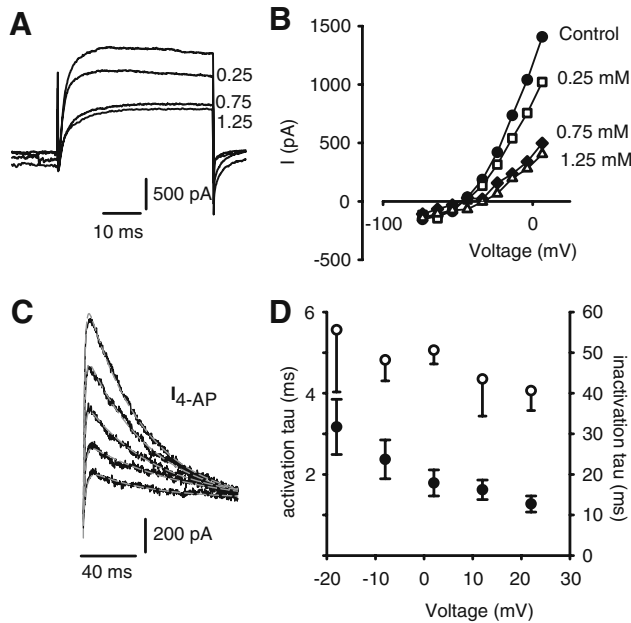


FIG. 5. 4-AP blocks a rapidly activating and inactivating outward current in calyx terminals. **A** Effect of different concentrations of 4-AP on outward currents. Control current during a step to +6 mV and currents during perfusion of 0.25, 0.75, and 1.25 mM 4-AP are shown. **B** IV relation showing reduction in peak currents with increasing 4-AP concentrations. Control (filled circles), 0.25 mM 4-AP (open squares), 0.75 mM 4-AP (filled diamonds), and 1.25 mM 4-AP (open triangles). **C** The 4-AP-sensitive current (I_{4-AP}) in another cell was obtained by subtracting the currents in response to voltage steps (120-ms duration) in 1.25 mM 4-AP from control currents. The rise time (activation) and decay (inactivation) of subtracted currents were each fitted with a single exponential (gray lines, Eq. 2). **D** The time constants of activation (mean \pm SEM, filled symbols, $n=7$) and inactivation of I_{4-AP} (unfilled symbols, $n=5$) are shown at five different voltages between -20 and $+30$ mV.

and finally to 1.25 mM. At steps to potentials between 0 and +5 mV following a 40-ms prepulse to -120 mV, the highest concentration of 4-AP that we used (2.5 mM) reduced peak current by $63.9 \pm 10.7\%$

(mean \pm SD, $n=8$, data not shown). We have previously shown that the block by 2.5 mM 4-AP is partly reversible (Rennie and Streeter 2006). The inactivating current blocked by 4-AP was studied during longer voltage steps (120-ms duration) as shown for another cell in Figure 5C. The 4-AP-sensitive current (I_{4-AP}) activated with rapid kinetics and showed substantial inactivation over the pulse (Fig. 5C). The activation and inactivation time courses of I_{4-AP} were each fitted with a single exponential, and mean values were plotted as a function of membrane potential as shown in Figure 5D. The time constant for activation of I_{4-AP} was voltage-dependent and decreased with depolarization (filled circles). The mean activation time constant was 2.37 ± 0.48 ms at -8 mV ($n=7$). The mean inactivation time constant of the 4-AP-sensitive current ranged from 40 to 55 ms and showed no clear voltage dependence (Fig. 5D, open circles).

In vestibular ganglion neurons, the K⁺ current sensitive to 4-AP was further separated into two components (Chabbert et al. 2001). One component of the 4-AP-sensitive current was blocked by 20 nM α -dendrotoxin (α -DTX) or 50 nM margatoxin. A second 4-AP-sensitive current was blocked by blood depressing substance (BDS-I, 250 nM) (Chabbert et al. 2001). α -DTX, a toxin isolated from the venom of mamba snakes, blocks K⁺ channels in the Kv1 family that contain the subunits Kv1.1, Kv1.2, Kv1.3, and Kv1.6 (Harvey 1997). In our experiments, α -DTX had no effect on outward currents in four calyces tested at concentrations up to 280 nM (data not shown), indicating that these channels are not prevalent in calyx terminals. The sea anemone toxin BDS-I was also tested and was found to block part of the outward current in calyces. Figure 6A shows the effect of 250 nM BDS-I on currents in a calyx terminal, and Figure 6B shows the peak outward current blocked in four calyces following BDS-I application. BDS-I is

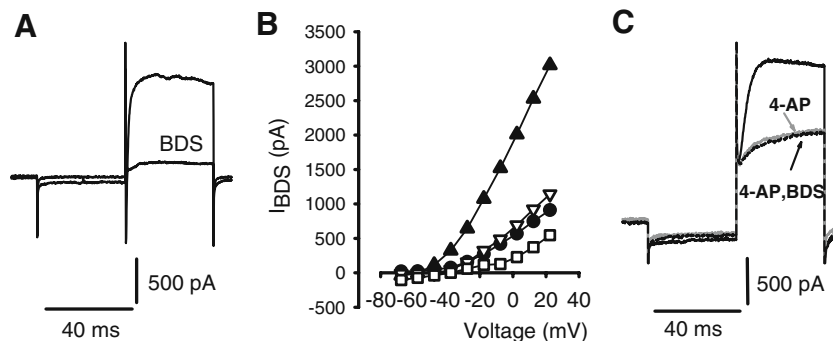


FIG. 6. The Kv3 channel blocker BDS-I blocked a component of the outward current. **A** Control current and reduced current in the presence of 250 nM BDS-I are shown. Currents were elicited during a voltage step to -18 mV. **B** BDS-I blocked outward current at potentials above -50 mV in four cells. The peak BDS-sensitive current (I_{BDS}) is shown vs. voltage, different symbols represent different cells. Concentrations of BDS-I were 40 nM (filled circles

and unfilled triangles), 200 nM (unfilled squares), and 250 nM (filled triangles). **C** Control current, current in the presence of 1.3 mM 4-AP (gray trace), and current in the presence of 1.3 mM 4-AP and 130 nM BDS-I (indicated by arrow) are shown. Currents were elicited during a voltage step to +32 mV. Addition of BDS-I did not produce a further block of current than that produced by 4-AP. The cell in this recording was a calyx terminal with a short segment of stalk.

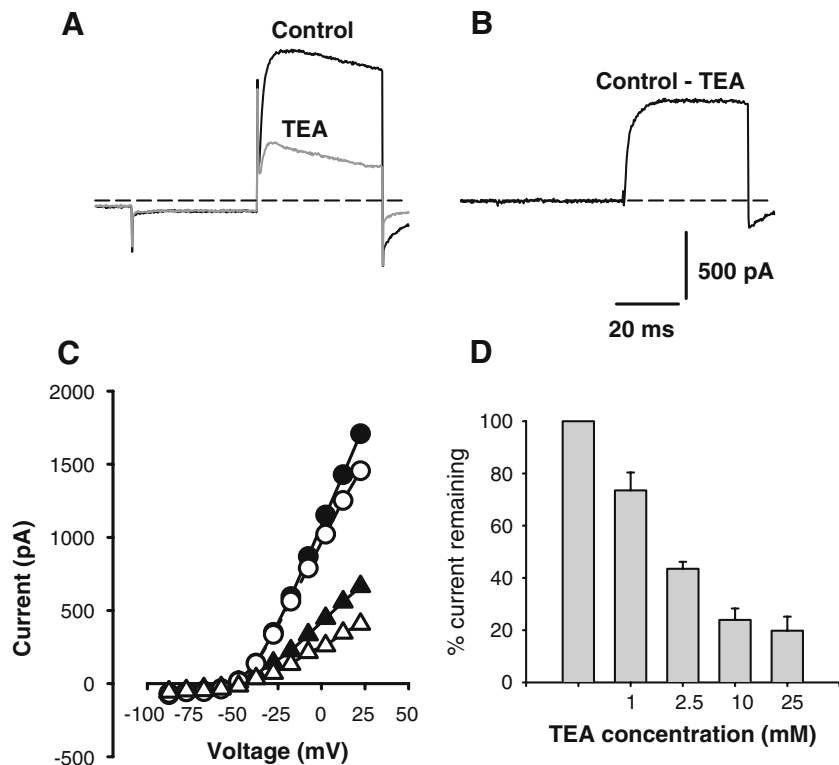


FIG. 7. Tetraethylammonium (TEA) blocks a slow outward current in calyx terminals. **A** Control current (black trace) for a 40-ms step to +2 mV following a 40-ms hyperpolarizing step to -128 mV from a holding potential of -78 mV in choline external solution. Reduced current following the same voltage step in the presence of 30 mM extracellular TEA/choline solution is shown in gray. The current blocked by TEA is shown in **B** and was obtained by subtracting the current in TEA from control current in **A**. **C** The peak current (filled circles) and current at the end of the 40-ms test pulse (unfilled circles) is compared to peak current (filled triangles) and current at the end of the pulse (unfilled triangles) in TEA. TEA blocks K⁺ current above approximately -40 mV. **D** Effect of increasing concentrations of TEA on outward currents. Current is expressed as a percentage of initial peak control current for 1 mM ($n=5$), 2.5 mM ($n=3$), 10 mM ($n=2$), and 25 mM ($n=4$) TEA.

reported to block Kv3 K⁺ channels which are associated with high-frequency firing in neurons (Yeung et al. 2005). To determine if 4-AP and BDS-I were blocking similar currents, 4-AP was applied to a cell followed by a combination of 4-AP and BDS-I (Fig. 6C). No additional current was blocked in the presence of 4-AP and BDS-I compared to 4-AP alone. This strongly suggests that the two drugs block the same set of channels in calyx terminals.

TEA block of outward K⁺ currents

Figure 7 shows the effect of a second K⁺ channel blocker, externally applied TEA, on the outward calyx current during a voltage step. Most of the TEA experiments were performed using external choline solutions, since we were concerned that changes in the extracellular Na⁺ solution, independent of TEA conditions, might alter outward currents as shown in Figure 3D. Figure 7A shows current in a choline-based extracellular solution (control) and current following application of 30 mM TEA/choline solution during a 40-ms test pulse. The current blocked by TEA was obtained by subtraction and is shown in Figure 7B. The TEA-sensitive current (I_{TEA}) activated slowly and did not inactivate over the 40-ms test pulse (Fig. 7B), whereas the current remaining in TEA showed substantial inactivation (Fig. 7A). The effect of 30 mM TEA on peak currents (filled symbols) and currents at the

end of the 40-ms pulse (unfilled symbols) is shown for a range of membrane potentials in the I - V plots of Figure 7C. Figure 7D shows the effect of different concentrations of TEA on the peak outward current. One millimolar TEA reduced the outward current by ~25%, and the block was maximal at 25 mM external TEA. This result is similar to that described by Chabbert et al. (2001), who found that a relatively high extracellular concentration of TEA (30 mM) was required to block a slowly activating voltage-gated current in vestibular ganglion cells.

The kinetics of I_{TEA} were considerably slower than I_{4-AP} (Fig. 7B). The activation time course of I_{TEA} was fitted with a single exponential with a mean value of 8.46 ± 0.7 ms at -8 mV ($n=4$) and was statistically significantly different from values for I_{4-AP} (t test, $P < 0.001$). Although no obvious time-dependent inactivation of I_{TEA} was evident during 40-ms test pulses, I_{TEA} demonstrated a slow inactivation during longer pulses as demonstrated in Figure 8B. The inactivation time constant of I_{TEA} was also much slower than that of I_{4-AP} and ranged from 150 to 600 ms at voltages between -28 and +22 mV.

Inactivation of K⁺ currents

To test whether TEA and 4-AP were selectively blocking separate populations of K⁺ channels, the two drugs were applied sequentially to single cells as shown for one cell in Figure 8A, B. 4-AP (2.5 mM)

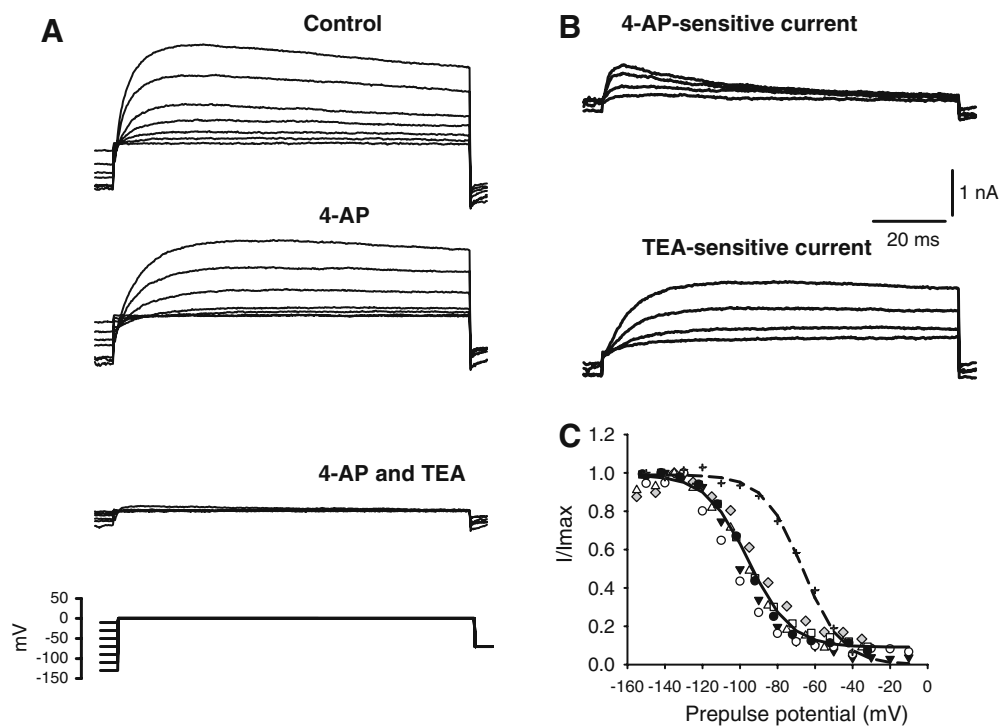


FIG. 8. Inactivation of 4-AP- and TEA-sensitive currents. **A** Conditioning pulses (150-ms duration) were applied before stepping to the test potential at 0 mV (100-ms duration) (voltage protocol shown in lower trace). Currents were recorded following perfusion of 2.5 mM 4-AP followed by a combination of 2.5 mM 4-AP and 25 mM TEA. **B** The 4-AP-sensitive current and the TEA-sensitive current both show voltage-dependent inactivation, but the 4-AP-

sensitive current has faster kinetics than the TEA-sensitive current. **C** Inactivation of the TEA-sensitive current as a function of prepulse potential. Conditioning pulses were 500-ms duration. Inactivation of I_{4-AP} from a different cell is included for comparison (*plus symbols*). A Boltzmann fit represented by *dashed line* gave a half-inactivation of -66.4 mV and S value of 10.5 mV.

was applied first and produced a reduction in outward current. This was followed by a combination of 25 mM TEA and 2.5 mM 4-AP, which led to a further reduction of the current (lower panel Fig. 8A). Indeed, the peak outward current was blocked $\sim 90\%$ by the combination of the two drugs.

Drug-sensitive components were obtained by subtracting the currents in the presence of the drug from the control currents to reveal the current components that were blocked by either 4-AP or TEA (Fig. 8B). The kinetics of the two blocked currents are clearly distinct; Whereas the 4-AP-sensitive current activated rapidly and declined after reaching a peak value, the TEA-sensitive current showed a slower activation and very slow inactivation over the 120-ms duration test step. Similar results using the combined drugs were seen in a total of four calyces, with the combination of TEA and 4-AP blocking on average $87.7 \pm 8.4\%$ (mean \pm SD) of the peak outward current at potentials above 0 mV.

The steady-state inactivation of I_{4-AP} and I_{TEA} were also examined using voltage protocols like the one shown in Figure 8A (bottom panel). First the voltage-dependent inactivation of the macroscopic K⁺ current was assessed by prepulsing the membrane to different

potentials before the test step. In this example, the cell membrane was stepped to a range of conditioning potentials for 150 ms before stepping to the test potential at -8 mV. Conditioning pulses to the most negative potentials resulted in the largest outward currents at the test step as shown in the upper panel of Figure 8A. The outward current was maximally activated following prepulses to potentials more negative than -110 mV. The steady-state inactivation plots for I_{TEA} are shown in Figure 8C and were fitted with a single Boltzmann function. Conditioning pulses of 500-ms duration were used to make I_{TEA} inactivation plots, since the extent of inactivation of I_{TEA} was noticeably greater when 500-ms conditioning pulses were used as compared to 150-ms conditioning pulses. It was not possible to assess the effect of conditioning pulses greater than 500-ms duration, since cells did not tolerate the longer pulses. The mean half-inactivation voltage ($V_{1/2}$) for I_{TEA} was -95.4 ± 1.4 mV and S was 11.3 ± 1.3 mV ($n=6$), and the extent of inactivation of I_{TEA} was up to $\sim 90\%$ (Fig. 8C). In contrast, the mean $V_{1/2}$ for I_{4-AP} was -70.8 ± 6.1 mV and S was 25.3 ± 3.9 mV ($n=5$). The steady-state inactivation plot and fit for the 4-AP-sensitive current in one cell is shown by the symbols

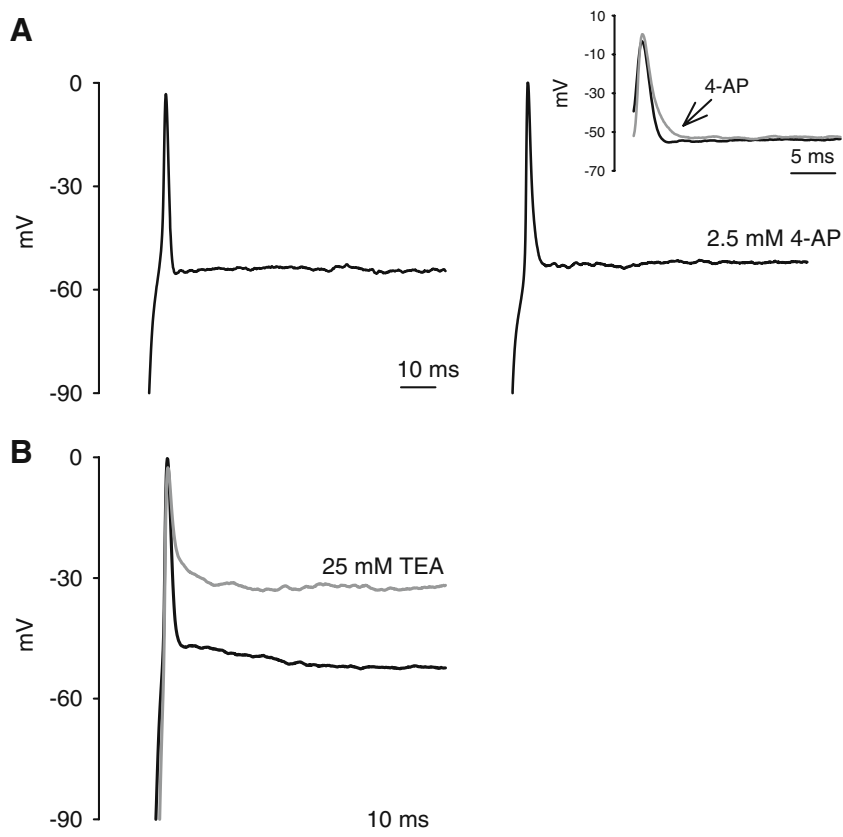


FIG. 9. Effects of K⁺ channel blockers on calyx action potentials recorded in current clamp. Action potentials were elicited by injecting constant current to hyperpolarize the membrane potential (removing Na⁺ channel inactivation) and then applying a current step. **A** A control action potential is shown on the *left* and an action potential in the same cell following 4-AP application is shown on the *right*. As shown in the *inset*, where the two waveforms are plotted together, the main effect of 4-AP was to slow the late falling phase of the action potential, therefore increasing spike width and to depolarize the cell membrane by only a few millivolts. **B** An action potential in control conditions (*black trace*) and following TEA perfusion (*gray trace*) is shown. The action potential fails to repolarize completely in 25 mM TEA during the current step, and the membrane potential (not shown) was ~15 mV less negative after the current step.

and dashed line to the right of the TEA data in Figure 8C.

Effects of 4-AP and TEA on action potentials

The average zero-current potential that we measured in calyx terminals in current clamp was -59.6 ± 1.1 mV (mean \pm SEM, $n=50$). There was no spontaneous firing at rest, but solitary action potentials could be recorded after injecting current to hyperpolarize the membrane to potentials more negative than approximately -80 mV as shown in Figure 9. Similarly, in somas of vestibular ganglion cells, spontaneous firing was not seen in whole-cell patch-clamp recordings, and action potentials were only evoked by current injections (Limón et al. 2005; Risner and Holt 2006; Iwasaki et al. 2008). These data are in contrast to intracellular and extracellular microelectrode recordings which have demonstrated spontaneous firing in vestibular afferents (Baird et al. 1988; Holt et al. 2007a; Lysakowski et al. 1995). Previous results have indicated that the half-inactivation voltage for the Na⁺ current in calyx terminals is quite negative, with a mean value of -83 mV (Rennie and Streeter 2006). This is more negative than the $V_{1/2}$ of the Na⁺ current in

vestibular ganglion cells, which was reported to be between -65 and -70 mV (Chabbert et al. 1997; Risner and Holt 2006). Membrane hyperpolarization below the zero-current potential is therefore needed to remove Na⁺ channel inactivation and allow action potentials to be evoked in calyx terminals. To determine the role of K⁺ channels in action potential shaping, the effects of K⁺ channel blockers on single evoked action potentials in calyces were examined as shown in Figure 9. Step current injections of 100-ms duration were given following injection of constant current to hyperpolarize the membrane in current clamp. Action potentials were observed as the cell membrane depolarized to the threshold for Na⁺ current activation, which was between -60 and -50 mV. The amplitude of the action potential was measured as the voltage change from threshold to peak and ranged from 47 to 76 mV. As shown in Figure 9A, 4-AP (2.5 mM) slowed the falling phase (*inset*) and increased the width of the action potential. The effect of TEA is shown on an action potential in another cell in Figure 9B. TEA slowed the falling phase and prevented the full repolarization of the action potential, consistent with the slower activation and inactivation of I_{TEA} .

DISCUSSION

Synaptic transmission between hair cells and their afferent terminals occurs at highly specialized ribbon synapses (Nouvian et al. 2006). Hair cell receptor potential changes produce graded release of neurotransmitter (glutamate) and modulation of action potential activity in the postsynaptic terminal. Although much is known about the membrane properties of type I and type II vestibular hair cells (Rennie and Correia 1994; Rennie et al. 1996; Rüscher et al. 1998; Chen and Eatock 2000; Hurley et al. 2006; Holt et al. 2007b), we know less about primary vestibular neurons which carry sensory information to the central nervous system as a discharge of action potentials. Of particular interest is the unusual calyx terminal which surrounds the basolateral membrane of one or more type I hair cells. It is not clear how AMPA-mediated receptor potentials drive action potentials in calyx fibers. We have characterized voltage-gated K⁺ conductances in mature vestibular calyces and recorded single-action potentials in these unmyelinated terminals. The role of K⁺ conductances in shaping afferent responses is discussed below.

4-AP-sensitive K⁺ current

We identified a rapidly activating and inactivating K⁺ current in calyx terminals that is sensitive to 4-AP (I_{4-AP}). The kinetic and pharmacologic properties of I_{4-AP} are consistent with A-type currents, which regulate firing rate and shape spike waveforms in other neurons (Coetzee et al. 1999). I_{4-AP} made up ~60% of the peak outward current at depolarized potentials in calyx terminals. In current clamp, 4-AP broadened action potential width as cells repolarized less rapidly during the falling phase. We did not observe successive action potentials in isolated calyx terminals, but reduction of the transient I_{4-AP} would be expected to lower spike rate during repetitive firing.

A 4-AP-sensitive K⁺ current was described in early postnatal mouse vestibular ganglion neurons and was further separated into two components using α -DTX and BDS-I (Chabbert et al. 2001; Risner and Holt 2006). The low-threshold α -DTX-sensitive current activated at potentials above -60 mV, was maximally blocked by 0.5 mM 4-AP, and inactivated less than 20% (Chabbert et al. 2001). Calyx terminals lack a low-threshold current, and α -DTX had no effect on currents described here. In calyces, I_{4-AP} activated at potentials above -50 mV, was maximally blocked by ~1.3 mM 4-AP, and showed extensive inactivation. The activation time constant for I_{4-AP} in calyx terminals was 1–2 ms, similar to values reported for the 4-AP-sensitive currents in vestibular ganglion neurons (Chabbert et al. 2001). In addition, the rapidly activating, rapidly inactivating 4-AP-sensitive current

in ganglion neurons had a mean half-inactivation of -64 mV, close to the mean value in gerbil calyx terminals of -71 mV.

An inactivating component of the outward current was also sensitive to BDS-I, which inhibits Kv3 K⁺ channels. The current blocked by BDS-I appeared to be the same as the current blocked by 4-AP. BDS-I is reported to alter the gating kinetics and voltage dependence of Kv3 channels (Yeung et al. 2005), precluding a detailed analysis of I_{BDS} . Kv3 channels typically activate at high threshold, deactivate rapidly, and allow fast repolarization of action potentials.

TEA-sensitive K⁺ current

Most of the current remaining after block of I_{4-AP} was sensitive to application of extracellular TEA (25–30 mM, Fig. 8). The kinetic properties of I_{TEA} were found to be considerably slower than I_{4-AP} . A similar K⁺ current was described in vestibular ganglion cells and was blocked by relatively high concentrations of TEA (30–40 mM) (Chabbert et al. 2001). We probed the steady-state inactivation of I_{TEA} with 500-ms conditioning pulses and found a $V_{1/2}$ for inactivation of approximately -90 mV. Chabbert et al. used 10-s conditioning pulses to study inactivation of I_{TEA} and reported a $V_{1/2}$ of -62 mV. Differences in voltage protocols may account in part for the different $V_{1/2}$ values between preparations. I_{TEA} inactivated up to 85% in ganglion neurons and up to 90% in calyces.

K⁺ channels which are sensitive to 1 mM TEA include members of the Kv1 and Kv3 families and BK currents (Wang et al. 1998; Coetzee et al. 1999) and are unlikely to be major contributors to I_{TEA} in calyces. KCNQ channels may contribute to K⁺ currents in calyx afferents (Kharkovets et al. 2000; Hurley et al. 2006; Rennie and Streeter 2006). Based on sensitivity to the KCNQ channel blockers linopirdine and XE991, it has been suggested that KCNQ “M-like” channels may underlie calyceal K⁺ currents (Hurley et al. 2006; Rennie and Streeter 2006). The classical M current is a 4-AP-insensitive low-voltage-activated K⁺ current that activates slowly and does not inactivate (Robbins 2001). KCNQ2, 3, 4, and 5 can contribute to M currents. The sensitivity of KCNQ channels to externally applied TEA differs with subunit type (Hadley et al. 2000). Expressed KCNQ2 channels are highly sensitive to block by TEA with an IC_{50} of 0.3 mM. A tyrosine residue which is located close to the canonical GYG sequence confers the high TEA sensitivity on KCNQ2 homomers (Hadley et al. 2000). The IC_{50} values for KCNQ1 and KCNQ4 were reported to be less than 10 mM, but currents mediated by KCNQ3 and KCNQ5 channels were much less sensitive to TEA with IC_{50} values > 30 mM (Hadley et al. 2000; Schroeder et al. 2000). Calyx endings were reported to show no

staining with KCNQ3 antibodies in the rat utricle (Hurley et al. 2006), but KCNQ5 staining was reported in calyces and their afferent stalks at P4-P8 and also at P21 (Hurley et al. 2006). KCNQ4 labeling has also been described in vestibular afferent calyces and ganglion cells in rodents (Kharkovets et al. 2000; Rocha-Sanchez et al. 2007). In rat utricle, KCNQ4 expression was restricted to the inner face of calyx terminals at P21 (Hurley et al. 2006). However, given the high sensitivity of KCNQ4 channel homomers to TEA, it appears that KCNQ4 alone is not a good candidate for the I_{TEA} described here. Perhaps KCNQ4 coassembles with other subunits such as KCNQ5 to form a channel with relatively low TEA sensitivity. A further difference between I_{TEA} in calyces and KCNQ currents is that KCNQ-mediated currents do not generally inactivate (Robbins 2001). However, recent studies have shown that currents mediated by KCNQ4 and 5 are increased by hyperpolarizing prepulses, indicating that inactivation can occur (Seebohm et al. 2005; Jensen et al. 2007). We found substantial inactivation of I_{TEA} in calyces, and further experiments are needed to determine if inactivating KCNQ channels such as KCNQ4 and 5 contribute to I_{TEA} .

Comparison to preparations studied during postnatal development

In rodents, calyx terminals appear during the first postnatal week when ion channel complements in hair cells and postnatal afferents may change rapidly (Rüsch et al. 1998; Hurley et al. 2006; Wooltorton et al. 2007). K⁺ currents in vestibular ganglion cells have been studied during the early postnatal period (P0–P8) in mouse (Chabbert et al. 2001; Risner and Holt 2006). Hurley et al. (2006) made whole-cell recordings from calyces and/or stalks isolated from the postnatal rat utricle (P17–P22). A large negatively activating conductance was described in three out of four cells with a $V_{1/2}$ ranging from –63 to –80 mV. The current was blocked by XE991 and resembled the conductances $g_{K,n}$ in cochlear hair cells or $g_{K,L}$ in type I hair cells (Hurley et al. 2006). We did not find a large resting current in any of the calyces studied here or in calyces from gerbils at younger ages (postnatal days 4–13, unpublished data). The reasons for these differences are unclear but may be due to different dissociation techniques used and/or differences between the utricle and crista. Instead, we observed a high-input resistance (0.4–1.3 G Ω) in calyces patched with standard patch electrode solutions and in calyx recordings confirmed with fluorescent dye. Input resistance values in calyces were much higher than values in type I hair cells. The relatively high-input resistance of calyx terminals described here would readily allow small changes in hair cell transmitter

release to result in membrane potential changes and modulate the firing of action potentials in afferents.

Action potentials in calyx afferents

We are interested in how channels in calyx terminals shape synaptic responses and action potential firing in calyx units. Although previous sharp electrode studies have consistently reported spontaneous firing in vestibular afferent fibers (Goldberg 2000), we did not observe spontaneous action potentials in calyces in whole-cell recordings. Spontaneous release of neurotransmitter occurs from type I hair cells and results in EPSCs in calyx afferents (Rennie and Streeter 2006). However, isolated calyx terminals described here lack a myelinated axon that may contain additional ion channels necessary for repetitive firing of action potentials. The effects of channel blockers on single-action potentials in whole-cell recordings from vestibular ganglion neurons excised from mice have also been described (Risner and Holt 2006). Our results indicate that the voltage-dependent currents I_{4-AP} and I_{TEA} contribute in different ways to action potential repolarization in calyces. Blocking the rapidly activating, rapidly inactivating A-type current increased spike width, whereas blocking the slower current I_{TEA} prevented complete repolarization of the action potential.

Roles of Ca²⁺ and calcium-activated K⁺ channels

Differences in after-hyperpolarization potential slope may influence the regularity of firing in vestibular afferent neurons and a calcium-activated K⁺ (K(Ca)) current may contribute (Smith and Goldberg 1986). Limón et al. (2005) found a correlation between ganglion cell soma size and the expression of K(Ca) channels in neurons from the early postnatal rat vestibular ganglion. In large-diameter cells, the BK channel blocker iberiotoxin increased action potential duration and reduced adaptation of the action potential discharge. Although other K(Ca) channel types were present, specific blockers of these channels (apamin and clotrimazole) had no effect on action potential shape (Limón et al. 2005). The potential role of Ca²⁺ and K(Ca) channels in calyx action potential shaping remains to be investigated. As we learn more about the biophysical properties and molecular identity of ionic channels in calyces, mechanistic differences between irregularly and regularly firing vestibular afferents and the nature of information conveyed by these complex afferents to central pathways should be elucidated.

ACKNOWLEDGEMENTS

This work was supported by grants from the National Institute on Deafness and other Communication Disorders (DC008297), the American Hearing Research Foundation, Deafness Research Foundation, and the National Organization of Hearing Research Foundation to KJR. FLM was supported by training grant HD41697. We thank Kenneth Anderson and Michael Hall for excellent technical and workshop assistance and Timothy Benke and Gang Li for comments and helpful discussions.

REFERENCES

- AUTRET L, MECHALY I, SCAMPS F, VALMIER J, LORY P, DESMADRYL G (2005) The involvement of Cav3.2/ α 1H T-type calcium channels in excitability of mouse embryonic primary vestibular neurons. *J Physiol* 567:67–78
- BAIRD RA, DESMADRYL G, FERNÁNDEZ C, GOLDBERG JM (1988) The vestibular nerve of the chinchilla. II. Relation between afferent response properties and peripheral innervation patterns in the semicircular canals. *J Neurophysiol* 60:182–203
- BHATTACHARJEE A, KACZMAREK LK (2005) For K⁺ channels, Na⁺ is the new Ca²⁺. *TINS* 28:422–428
- BONSACQUET J, BRUGEAUD A, COMPAN V, DESMADRYL G, CHABBERT C (2006) AMPA type glutamate receptor mediates neurotransmission at turtle vestibular calyx synapse. *J Physiol* 576:63–71
- CHABBERT C, CHAMBARDE JM, VALMIER J, SANS A, DESMADRYL G (1997) Voltage-activated sodium currents in acutely isolated mouse vestibular ganglion neurones. *Neuroreport* 8:1253–1256
- CHABBERT C, CHAMBARDE JM, SANS A, DESMADRYL G (2001) Three types of depolarization-activated potassium currents in acutely isolated mouse vestibular neurons. *J Neurophysiol* 85:1017–1026
- CHAMBARDE JM, CHABBERT C, SANS A, DESMADRYL G (1999) Developmental changes in low and high voltage-activated calcium currents in acutely isolated mouse vestibular neurons. *J Physiol* 518:141–149
- CHEN JWY, EATOCK RA (2000) Major potassium conductance in type I hair cells from rat semicircular canals: characterization and modulation by nitric oxide. *J Neurophysiol* 84:139–151
- COETZEE WA, AMARILLO Y, CHIU J, LAU D, McCORMACK T, MORENO H, NADAL MS, OZAITA A, POUNTEY D, SAGANICH M, VEGA-SAENZ DE MIERA E, RUDY B (1999) Molecular diversity of K⁺ channels. *Ann NY Acad Sci* 868:233–285
- DESAI SS, HUSSAIN A, LYSAKOWSKI A (2005) Comparative morphology of rodent vestibular periphery. II. Cristae ampullares. *J Neurophysiol* 93:267–280
- FERNÁNDEZ C, BAIRD RA, GOLDBERG JM (1988) The vestibular nerve of the chinchilla. I. Peripheral innervation patterns in horizontal and superior semicircular canals. *J Neurophysiol* 60:167–181
- GOLDBERG JM (1996) Theoretical analysis of intercellular communication between the vestibular type I hair cell and its calyx ending. *J Neurophysiol* 76:1942–1957
- GOLDBERG JM (2000) Afferent diversity and the organization of central vestibular pathways. *Exp Brain Res* 130:277–297
- GULLEY RL, BAGGER-SJÖBACK D (1979) Freeze fracture studies on the synapse between the type I hair cell and the calyceal terminal in the guinea-pig vestibular system. *J Neurocytol* 8:591–603
- HADLEY JK, NODA M, SELYANKO AA, WOOD IC, ABOGADIE FC, BROWN DA (2000) Differential tetraethylammonium sensitivity of KCNQ1-4 potassium channels. *Br J Pharmacol* 129:413–5
- HARVEY AL (1997) Recent studies on dendrotoxins and potassium ion channels. *Gen Pharmacol* 28:7–12
- HOLT JC, CHATLANI S, LYSAKOWSKI A, GOLDBERG JM (2007A) Quantal and nonquantal transmission in calyx-bearing fibers of the turtle posterior crista. *J Neurophysiol* 98:1083–101
- HOLT JR, STAUFFER EA, ABRAHAM D, GÉLÉOC GSG (2007B) Dominant-negative inhibition of M-like potassium conductances in hair cells of the mouse inner ear. *J Neurosci* 27:8940–8951
- HURLEY KM, GABOYARD S, ZHONG M, PRICE SD, WOOLVERTON JRA, LYSAKOWSKI A, EATOCK RA (2006) M-like K⁺ currents in type I hair cells and calyx afferent endings of the developing rat utricle. *J Neurosci* 40:10253–10269
- IWASAKI S, CHIHARA Y, KOMUTA Y, ITO K, SAHARA Y (2008) Low-voltage-activated potassium channels underlie the regulation of intrinsic firing properties of rat vestibular ganglion cells. *J Neurophysiol* 100:2192–2204
- JENSEN HS, MORTEN G, OLESEN SP (2007) Inactivation as a new regulatory mechanism for neuronal Kv7 channels. *Biophys J* 92:2747–2756
- KHARKOVETS T, HARDELIN JP, SAFIEDDINE S, SCHWEIZER M, EL-AMRAOUI A, PETIT C, JENTSCH TJ (2000) KCNQ4, a K⁺ channel mutated in a form of dominant deafness, is expressed in the inner ear and the central auditory pathway. *Proc Natl Acad Sci* 97:4333–4338
- LIMÓN A, PÉREZ C, VEGA R, SOTO E (2005) Ca²⁺-activated K⁺-current density is correlated with soma size in rat vestibular-afferent neurons in culture. *J Neurophysiol* 94:3751–3761
- LYSAKOWSKI A, GOLDBERG JM (1997) Regional variations in the cellular and synaptic architecture of the chinchilla crista. *J Comp Neurol* 389:419–443
- LYSAKOWSKI A, MINOR LB, FERNÁNDEZ C, GOLDBERG JM (1995) Physiological identification of morphologically distinct afferent classes innervating the cristae ampullares of the squirrel monkey. *J Neurophysiol* 73:1270–1281
- NOUVIAN R, BEUTNER D, PARSONS TD, MOSER T (2006) Structure and function of the hair cell ribbon synapse. *J Membrane Biol* 209:1–13
- RENNIE KJ, CORREIA MJ (1994) Potassium currents in mammalian and avian isolated type I semicircular canal hair cells. *J Neurophysiol* 71:317–329
- RENNIE KJ, STREETER MA (2006) Voltage-dependent currents in isolated vestibular afferent calyx terminals. *J Neurophysiol* 95:26–32
- RENNIE KJ, RICCI AJ, CORREIA MJ (1996) Electrical filtering in gerbil isolated type I semicircular canal hair cells. *J Neurophysiol* 75:2117–2123
- RICCI AJ, RENNIE KJ, COCHRAN SL, KEVETTER GA, CORREIA MJ (1997) Vestibular type I and type II hair cells. 1: Morphological identification in the pigeon and gerbil. *J Vestib Res* 7:393–406
- RISNER JR, HOLT JR (2006) Heterogeneous potassium conductances contribute to the diverse firing properties of postnatal mouse vestibular ganglion neurons. *J Neurophysiol* 96:2364–2376
- ROBBINS J (2001) KCNQ potassium channels: physiology, pathophysiology and pharmacology. *Pharmacol Therap* 90:1–19
- ROCHA-SANCHEZ SMS, MORRIS KA, KACHAR B, NICHOLS D, FRITZSCH B, BEISEL KW (2007) Developmental expression of Kcnq4 in vestibular neurons and neurosensory epithelia. *Brain Res* 1139:117–125
- RÜSCH A, LYSAKOWSKI A, EATOCK RA (1998) Postnatal development of type I and type II hair cells in the mouse utricle: acquisition of voltage-gated conductances and differentiated morphology. *J Neurosci* 18:7487–7501
- SCHROEDER BC, HECHENBERGER M, WEINREICH F, KUBISCH C, JENTSCH TJ (2000) KCNQ5, a novel potassium channel broadly expressed in brain, mediates M-type currents. *J Biol Chem* 275:24089–24095
- SEEBOHM G, STRUTZ-SEEBOHM N, BALTAEV R, KORNYCHUK G, KNIRSCH M, ENGEL J, LANG F (2005) Regulation of KCNQ4 potassium channel prepulse dependence and current amplitude by SGK1 in *Xenopus* oocytes. *Cell Physiol Biochem* 16:255–262
- SMITH CE, GOLDBERG JM (1986) A stochastic afterhyperpolarization model of repetitive activity in vestibular afferents. *Biol Cybern* 54:41–51
- SOTO E, CERVANTES B, LIMÓN A, VEGA R (2006) Sodium activated potassium current participates in the action potential repolari-

- zation in the vestibular afferent-neurons of the rat. Abstract 759, ARO
- WANG LY, GAN L, FORSYTHE ID, KACZMAREK LK (1998) Contribution of the Kv3.1 potassium channel to high-frequency firing in mouse auditory neurons. *J Physiol* 509:183–194
- WERSÄLL J (1956) Studies on the structure and innervation of the sensory epithelium of the cristae ampullares in the guinea pig. A light and electron microscopic investigation. *Acta Otolaryngol Suppl* 126:1–85
- WOOLTORTON JRA, GABOYARD S, HURLEY KM, PRICE SD, GARCIA JL, ZHONG M, LYSAKOWSKI A, EATOCK RA (2007) Developmental changes in two voltage-dependent sodium currents in utricular hair cells. *J Neurophysiol* 97:1684–1704
- YEUNG SY, THOMPSON D, WANG Z, FEDIDA D, ROBERTSON B (2005) Modulation of Kv3 subfamily potassium currents by the sea anemone toxin BDS: significance for CNS and biophysical studies. *J Neurosci* 25:8735–8745